Design and Implementation of a Pillbox Antenna for an Airborne Imaging Radar

S.B. Gambahaya, M.R. Inggs
Radar Remote Sensing Group, Department of Electrical Engineering
University of Cape Town, Private Bag, Rondebosch 7701, South Africa
Email: mikings@ebe.uct.ac.za Web: http://www.rrsg.uct.ac.za
Tel: +27 21 650 2799 Fax: +27 21 650 3465

June 23, 2006

Abstract

This paper describes the design and implementation of the fan beam radar antenna for SASAR II. The SASAR II project is an ongoing initiative to demonstrate the capability of South Africa to produce high quality imagery using (SAR) Synthetic Aperture Radar techniques. The Radar Remote Sensing Group (RRSG) at UCT was commissioned by Denel Aviation Systems, SunSpace, and UCT to design, implement and test a high resolution X-band SAR, as a follow-on to the successful VHF Radar developed and flown in 2000. The antenna was to be able to radiate through a cabin window of an Aerocommander aicraft. The antenna specifications were determined from image signal processing requirements [12]. The pillbox was chosen due to its relative simplicity in design and analysis. MATLAB simulations were carried out to predict the radiation characteristics of the antenna. The fully fabricated antenna was then tested and comparisons were made between the actual performance of the antenna and theoretical predictions. This paper has been written as a tutorial, and contains some detailed information of testing using relatively primitive antenna test facilities.

1 Introduction

A pillbox antenna is a linearly polarized cylindrical reflector embedded between two parallel plates. It is usually fed by a waveguide [9] [19]. The pillbox is part of a family of antennas called fan beam antennas which produce a wide beam in one plane and a narrow beam in the other [15] [19].The pillbox antenna can be dual-polarized and is also a relatively wide bandwidth antenna. The pillbox antenna has existed for at least fifty years and it was used for military surveillance radars during the Second World War and just after the Second World War [19]. The British version was called the cheese antenna. The primary difference between the cheese antenna and the pillbox is the separation of the parallel plates and their possible modes of electromagnetic propagation [9] [19]. The following requirements were specified for the radar antenna of the SAR system by the system engineer [10] [11] [12].

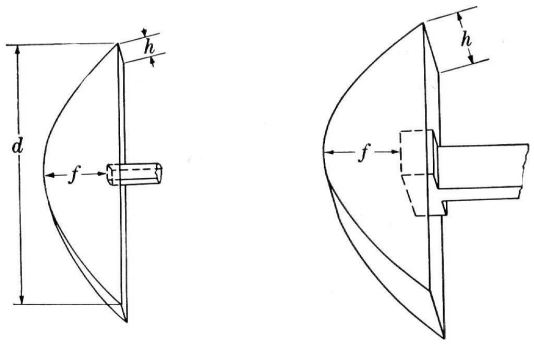

Figure 1: Pillbox or Cheese Antenna (from [19]).

1. A pillbox antenna with a single mode of propagation is to be designed, implemented and tested to meet specifications. If several modes can propagate simultaneously, there is no control over which mode actually contains the transmitted signal, thus causing dispersions, distortions and erratic opera-

tion [16].

2. The operating centre frequency is set to $\mathrm{f}_{\circ} = 9.3$ GHz.

3. The antenna operating bandwidth which is determined by the transmitter is $\mathrm{B} = 100$ MHz.

4. The antenna 3 dB azimuth beamwidth shall be 3.8° and the elevation beamwidth shall be 25°.

5. The peak power that the antenna system can handle is 3.5 kW.

6. The antenna should be able to operate at a platform height of 3000-8000 m. The aircraft cabin is pressurised at the equivalent of 8000 feet. The antenna shall be mounted inside the aircraft, pressing against the perspex window, to avoid costly airframe modifications.

The advantages of using a pillbox antenna for radar applications are given below [19]

- It is easy to design and the cost of production is low.
- It is dually-polarized and it is also a wide band antenna.
- It has a high power handling capability.

2 Design of Antenna

2.1 Design Theory

The pillbox design was based on the aperture field method as well as diffraction theory of aperture antennas. By using geometrical optics [6] and the diffraction theory of antennas we can predict the far-field of an antenna. There is a Fourier Transform relationship between the far-field and the aperture field which is analogous to the relationship between Fourier spectra and time domain waveforms (even though waveforms are one-dimensional). The far-field can be predicted by taking the Fourier Transform of the tangential component of the E-field. This one dimensional treatment is adequate for discussing the pillbox antenna since its directivity can be separable into a product of directivities of one-dimensional apertures made up of the length and width of the aperture [3]. Once the aperture fields are have been calculated, we use equation 1 to predict the far-field pattern of the antenna in the E and H-planes [5] [6][7]:

$$\mathrm{E}(\theta) = \int_{-\mathrm{x}/2}^{\mathrm{x}/2} \mathrm{f}(\mathrm{x})\, e^{\mathrm{jk}\mathrm{x}\sin\theta} \mathrm{dx} \qquad (1)$$

Where
$\mathrm{f}(\mathrm{x})$ is the aperture field distribution function across the aperture, 'x' is the length of the aperture and 'k' is the wavenumber.

2.2 Offset fed Pillbox Design

Offset prime-focus-reflectors are desirable because of the ability to offset the feed enough so that it is not in the way of the aperture to cause aperture blockage which consequently raises the sidelobe levels. However, offset-fed reflectors with a linearly polarized feed suffer from higher cross-polarization than axisymmetric reflectors [20]. Here the major design emphasis is on the choice of offset angle or feed pointing angle ψ_{f} to reducing sidelobe levels and also reduce cross polarization without a sacrifice in gain [20].

Offset reflector antennas inherently produce off-axis cross-polarization in the principal plane normal to the offset plane. The cross-polarization is a result of the asymmetric mapping of the otherwise symmetrical pattern into the aperture antenna [2] [18]. We wish to keep the cross-polarization levels to at least 30 dB below the peak of the co-polar pattern for satisfactory performance of the antenna [15][18].

2.2.1 The Geometry

The geometry of the offset fed configuration is shown in figure 2. The primary parameters that we can control are the degree of offset by varying h and the aiming of the feed antenna $(\text{the angle } \psi)$. In this paper we consider the case of the more than fully offset feed, $\mathrm{h} > 0$ to provide a blockage-free region for the structures in the focal region. In practice in order to keep spill-over losses reasonable the feed is aimed within the range [19] [20]:

$$40^{\circ} \leq \quad \psi_{\mathrm{f}} \leq \quad 60^{\circ}$$

The definitions of the symbols used in Figure 2 are given below where

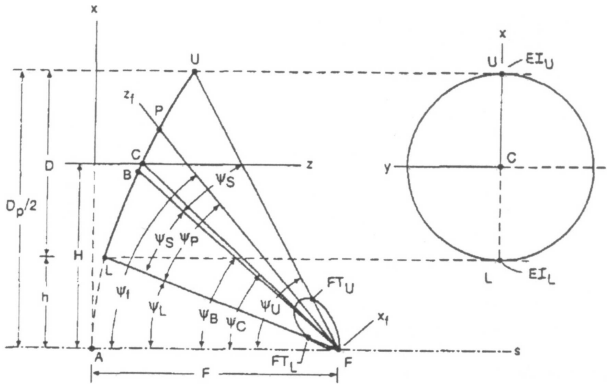

Figure 2: Offset Parabolic Reflector Geometry (from [20])

D	=	Diameter of the projected aperture of the cylindrical reflector
h	=	Offset distance
$\mathrm{D_p}$	=	Diameter of the projected aperture of the parent paraboloid.
F	=	Focal length.
$\mathrm{f/D_p}$	=	'$\mathrm{f/D}$' of parent reflector.
ψ_f	=	Angle of antenna pattern peak relative to reflector axis of symmetry
ψ_c	=	Value of ψ_f when the feed is aimed at the aperture centre.
ψ_E		Value of ψ_f when the feed yields an equal edge illumination .
ψ_f	=	Value of ψ_f which bisects the reflector subtended angle.
FT	=	Feed edge taper; $\mathrm{FT} \geq 0$.
EI	=	Edge illumination; $\mathrm{EI} = -(\mathrm{FT} + \mathrm{SPL})$; SL is the spherical spread loss.

The spherical spread loss of the antenna is given by [20] :

$$\mathrm{SPL}\left(\psi\right) \quad = \quad -20\log\left[\cos^2\frac{\psi}{2}\right] \qquad (2)$$

Quoting 'W. Stutzman', several numerical simulations using the physical optics computer code $GRASP{-}7$ on reflector antennas yielded the following results [20]:

- " Several numerical simulations showed that the orientation of the feed strongly influences cross-polarization. In particular small feed pointing angles lead to high spillover which would raise the sidelobe and cross-polarization levels for a high gains.
- Large $\mathrm{f/D_p}$values which lead to reduced feed pointing angles ψ_f cause degradation in sidelobe levels even though the cross-polarization level improves. Based on the above observations, we can thus try to optimize the feed pointing or offset angle to yield the lowest sidelobes and cross-polarization levels with the smallest penalties in gain. A feed pointing angle of $\psi_\mathrm{f} = \psi_\mathrm{E}$ achieves this specification and it also turns out that this operating point produces a balanced aperture illumination, that is the edge illumination levels (in the plane of offset) in the aperture are equal ".

The diameter of the parent parabola was fixed at $\mathrm{D_p} = 126$ cm and curvature of the reflector was $\mathrm{f/D_p} = 0.3$ to achieve a good compromise between sidelobe levels and cross-polarization. The design presented here was a single polarisation version, to simplify the feed horn design.

2.2.2 Reflector Aperture Dimensions

We calculated the angles ψ_L and ψ_U which are the angles subtended by the lower and upper edges of the reflector respectively using equation 3 [2][16] [19] :

$$\rho\left(\psi\right) \quad = \quad 2\mathrm{f}\tan\left(\frac{\psi}{2}\right) \qquad (3)$$

- The angle subtended by the upper edge of the reflector is calculated as follows:

$$\begin{aligned}\psi_\mathrm{U} &= 2\cdot\arctan\left(\frac{64}{2\times 38}\right)\\ &\approx 80^\circ\end{aligned}$$

- The angle subtended by the lower edge of the reflector is calculated as follows:

$$\begin{aligned}\psi_\mathrm{L} &= 2\cdot\arctan\left(\frac{7}{2\times 38}\right)\\ &\approx 11^\circ\end{aligned}$$

Where ρ is the perpendicular distance from the parent reflector centre to the upper edge. The feed pointing

angle was $\psi_{\mathrm{B}} = 45^{\circ}$. A simple MATHCAD calculation gave the length of the feed horn in the offset plane to achieve an equal edge illumination of approximately -10 dB at the edges. The length of the horn was calculated to be 6.5 cm. It was only later discovered that there was an error in the initial calculation of the horn azimuth dimension, it should have been 6 cm instead.

- The additional taper due to the space loss in ψ_{L} is small and can be neglected. The SL at ψ_{U} is calculated as follows:

$$\begin{aligned} \mathrm{SPL_U} &= -20\log\left[\cos^2\left(\frac{80}{2}\right)\right] \\ &= 4.5 \ [\mathrm{dB}] \end{aligned} \tag{4}$$

The space loss will introduce an additional 4.5 dB taper in the secondary aperture field distribution at the upper edge of the reflector.

- The length $\mathrm{D_{az}}$ of the aperture required to produce an edge illumination of -10 dB at the reflector edges is calculated by the following equation [16] [19]:

$$\begin{aligned} \mathrm{D_{az}} &= \left(1.05\mathrm{A_{edge}} + 55.95\right)\frac{\lambda}{\theta_{\mathrm{az}}} \\ &= \left((1.05^{\circ}\times 10) + 55.95\right)\frac{3.2}{3.8} \\ &= 56 \ [\mathrm{cm}] \end{aligned} \tag{5}$$

- The width of the aperture for a uniform illumination in the elevation plane is calculated by the following equation:

$$\begin{aligned} \mathrm{D_{el}} &= \frac{57\lambda}{\theta_{\mathrm{el}}} \\ &= \frac{57\times 3.2}{25} \\ &= 7 \ [\mathrm{cm}] \end{aligned} \tag{6}$$

- The offset distance was set to $\mathrm{h} = \mathrm{D}/8$ so that '$\mathrm{h} = 7\,\mathrm{cm}$'.

2.2.3 Directivity of Pillbox Antenna

$$\begin{aligned} \mathrm{G_D} &\approx \frac{1}{\mathrm{k}}\cdot\frac{4\pi}{\theta_{\mathrm{az}}\cdot\theta_{\mathrm{ele}}} \\ &= \frac{4\pi}{0.44\times 0.066\times 1.12} \\ &= 25.6 \ [\mathrm{dBi}] \end{aligned} \tag{7}$$

where $\theta_{\mathrm{az}}$and θ_{ele} are the principal azimuth and elevation beamwidths respectively, 'k' is the beam broadening factor relative to a uniform distribution, which is also the loss in directivity. The value of k=0.44 was approximated from the taper imposed on the upper edge of the parabolic reflector relative to a uniform distribution. The gain of an antenna which includes the directivity and power gain are well documented in [1].

2.2.4 Aperture Field Method:Predicted Azimuth Pattern

We used the aperture field method to determine the offset reflector pattern in the azimuth plane at $\psi_{\mathrm{f}} = 45^{\circ}$. We evaluated the equivalent Huygens sources at the aperture and integrated these sources to obtain the reflector far-field pattern[2][9] [14]. This section shows the steps taken to predict the reflector far-field.

The equation of the parabolic cylinder in polar coordinates is given as [6]:

$$\begin{aligned} \rho\left(\psi\right) &= \frac{\mathrm{f}}{\cos^2\left(\psi/2\right)} \\ &= \frac{2\mathrm{f}}{1+\cos\psi} \end{aligned} \tag{8}$$

The primary and secondary power flows are equal and given as [6]:

$$\mathrm{P\left(y\right)} = \mathrm{I}\left(\psi\right)\,\mathrm{dy} \tag{9}$$

where $\mathrm{I_{az}}\left(\psi\right)$ is the feed far-field power pattern of the horn in units of watts per radian-meter. $\mathrm{P\left(y\right)}$ is the secondary power flow in units of watts per radian-meter.

The feed radiation pattern in the H-plane is modelled by the following Fourier Transform expression at the feed pointing angle $\psi_{\mathrm{f}} = 45^{\circ}$ [9]:

$$\mathrm{E_{az}}\left(\psi-\psi_{\mathrm{offset}}\right) = \int_{-\mathrm{a_1}/2}^{\mathrm{a_1}/2}\mathrm{E_0}\cos\left(\frac{\pi\mathrm{x}}{\mathrm{a}}\right)e^{j\alpha}\mathrm{dx}$$

where

$$\alpha = \frac{2\pi}{\lambda}\mathrm{x}\sin\left(\psi - \psi_{\mathrm{offset}}\right) \quad (10)$$

The azimuthal power pattern of the horn is given by:

$$\mathrm{I_{az}}\left(\psi\right) = \mathrm{I_{az}^2}\left(\psi - \psi_{\mathrm{offset}}\right) \quad (11)$$

The equation relating the primary and secondary power distributions is given by the following expression [6]:

$$\begin{aligned}\mathrm{P}\left(y\right) &= \frac{\mathrm{I}\left(\psi\right)}{\rho\left(\psi\right)} \quad (12)\\ &= \frac{\mathrm{I_{az}}\left(\psi\right)\cos^2\left(\psi/2\right)}{\mathrm{f}}\end{aligned}$$

The aperture field of the reflector is given by the following expression [6]:

$$\mathrm{f_{az}}\left(\mathrm{y}\right) = \mathrm{P}\left[\left(\mathrm{y}\right)\right]^{1/2} \quad (13)$$

The far-field pattern of the reflector is then given by the following Fourier Transform expression [6]:

$$\mathrm{F_{az}}\left(\psi\right) = \int_{-\mathrm{D_{az}}/2}^{\mathrm{D_{az}}/2} \mathrm{f_{az}}\left(\mathrm{y}\right) e^{j\frac{2\pi}{\lambda}y\sin\psi}\mathrm{dy} \quad (14)$$

Where h = Offset distance = distance from the axis of symmetry(ies) to the lower reflector edge. $\mathrm{D_{az/2}}$ is half the span of the parent parabola.

2.2.5 Predicted Elevation Pattern

Assuming **the tangent plane approximation of physical optics** [5], we can predict the elevation pattern by the following expression:

$$\mathrm{E_{el}}\left(\psi\right) = \int_{-\mathrm{D_{el}}/2}^{\mathrm{D_{el}}/2} \mathrm{E_o} e^{j\frac{2\pi}{\lambda}y\sin\psi}\mathrm{dy} \quad (15)$$

Where $\mathrm{D_{el}}/2 \leq h \leq -\mathrm{D_{el}}/2$ is the height of the pillbox aperture.

The power radiation pattern in the vertical plane is given by [9] :

$$\mathrm{P_{el}}\left(\theta\right) = \mathrm{E_{el}^2}\left(\theta\right) \quad (16)$$

2.3 Design of Feed Horn

A pyramidal horn can only be constructed for dimensions that satisfy the following equation [2] [13]:

$$\left(\mathrm{a_1} - \mathrm{a}\right)^2\left[\left(\frac{\rho_\mathrm{h}}{\mathrm{a_1}}\right)^2 - \frac{1}{4}\right] = \left(\mathrm{b_1} - \mathrm{b}\right)^2\left[\left(\frac{\rho_\mathrm{e}}{\mathrm{b_1}}\right) - \frac{1}{4}^2\right] \quad (17)$$

The dimension of the horn to achieve a -10 dB edge illumination in the azimuth planes was calculated in MATHCAD and found to be $\mathrm{a_1} = 6.0$ cm. The $\mathrm{TE_{1,0}}$ waveguide dimension $\mathrm{a} = 2.286$ cm. In the elevation plane the horn dimension $\mathrm{b_1}$ is determined by the separation of the plates, therefore $\mathrm{b_1} = 7$ cm. The $\mathrm{TE_{1,0}}$ waveguide dimension $\mathrm{b} = 1.016$ cm.

- We chose a flare angle of 20° in the E-plane and using simple trigonometry, the slant length in the E-plane is calculated as follows:

- By making use of equation 17 and making ρ_h the subject of the formula, the slant length in the H-plane is calculated as follows:

$$\begin{aligned}\left(\mathrm{a_1} - \mathrm{a}\right)^2\left[\left(\frac{\rho_\mathrm{h}}{\mathrm{a_1}}\right)^2 - \frac{1}{4}\right] &= \left(\mathrm{b_1} - \mathrm{b}\right)^2\left[\left(\frac{\rho_e}{\mathrm{b_1}}\right)^2 - \frac{1}{4}\right]\\ \left(\frac{\rho_\mathrm{h}}{6.5}\right)^2 &\approx 4.055\\ \rho_\mathrm{h} &= 13.09\ [\mathrm{cm}] \quad (18)\end{aligned}$$

- From simple trigonometry, $\rho_h = 13.09$ cm corresponds to an H-plane flare angle calculated as:

$$\begin{aligned}\psi_\mathrm{h} &= \arcsin\left(\frac{3.25}{13.09}\right)\\ \psi_\mathrm{h} &= 14.5^\circ \quad (19)\end{aligned}$$

2.4 Antenna Construction

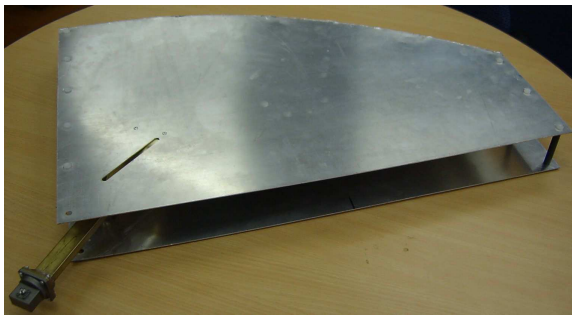

Figure 3: Top View of Fully Constructed Antenna

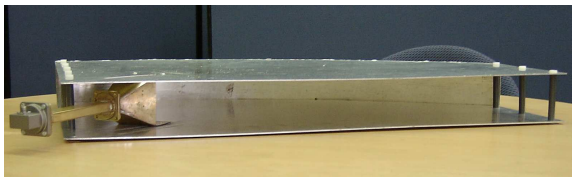

Figure 4: Front View of Fully Constructed Antenna

The feed horn was made out of brass of 1 mm thickness and the parallel plates as well as the cylindrical reflector were made out of 2mm thick aluminium. The key aspects in the manufacturing of the antenna prototype are listed below:

- The plates had to be flat with no bending as this might excite modes other than TEM.
- The feed positioning is important and in this regard it was designed so that it was embedded between the parallel plates and made movable back and forth so as to locate the phase centre. Plastic screws were used to fasten the feed in place.
- We avoided vertical walls on either side of the pillbox as these might cause internal reflections and affect performance as well as possibly short out the E field and cause propagation of higher modes. Instead we used PVC dielectric posts to support the parallel plates and maintain rigidity.
- Any gaps between the plates and the reflector were avoided as this would cause radiation leakage and this might affect the far-field pattern and gain measurements. However we assumed that tiny gaps created by bending the reflector should not affect our readings significantly.

3 Results

3.1 Return Loss

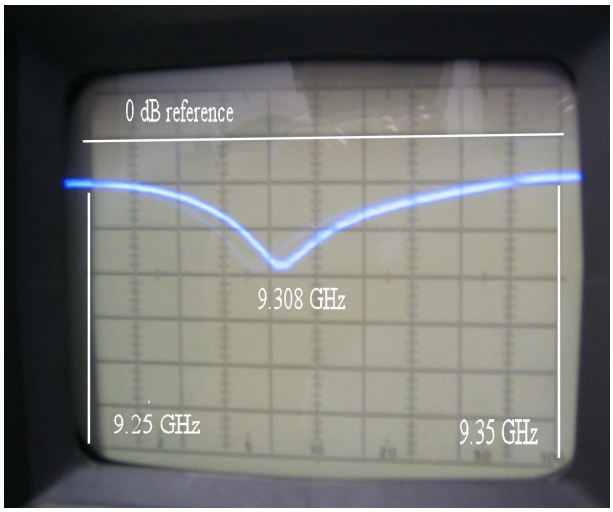

Figure 5: Return Loss Plot

The return loss or S_{11} is indicative of the fraction of the incident power reflected back to the feed over a frequency range of measurement and is given by [4] [17]:

$$\begin{aligned} \mathrm{RL\,(dB)} &= -20\log\mid\tau\mid \qquad (20) \\ &= 20\log\left|\frac{1}{S_{11}}\right| \end{aligned}$$

The impedance bandwidth of the antenna was calculated for a VSWR ≤ 2 [4][17]. There was a good impedance match between the transmitter and the antenna for a return loss of 10 dB or more in the 100 MHz (9.25-9.35 GHz) frequency band of interest. The impedance bandwidth was measured from Figure 5 and found to be approximately 100 MHz which was the same as the transmitter bandwidth.

3.2 Simulation Results:

Figure 6 shows the MATLAB simulation of the E-plane (elevation) pattern of the feed horn. The beamwidth

was found to be approximately 25°. The first sidelobes were at a level of -13 dB.

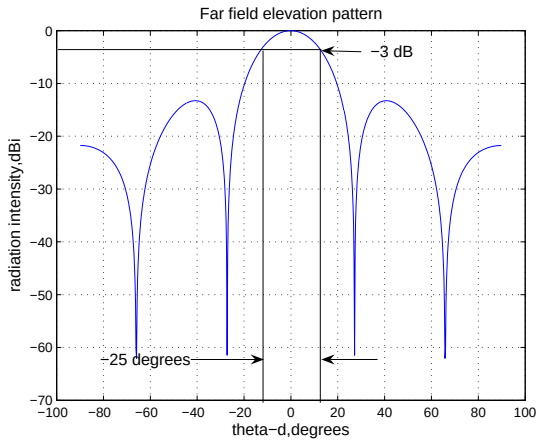

Figure 6: E-plane Feed Horn Pattern

Figure 7 shows the H plane pattern (azimuth pattern) of the feed horn at a feed pointing angle of 45°. The 3 dB beamwidth is approximately 37°. The largest sidelobes were at a level of approximately -21 dB.

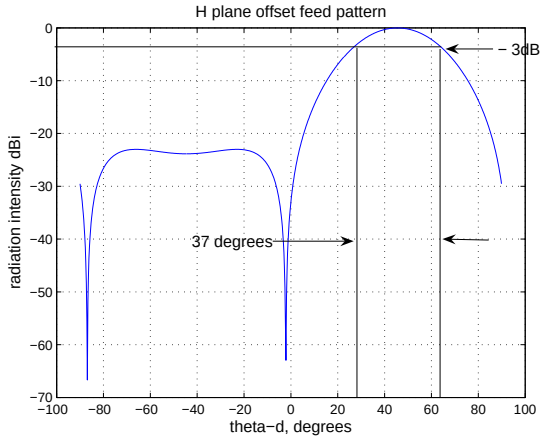

Figure 7: H-plane Pattern of Feed Horn (offset feed)

Figure 8 shows the MATLAB simulation of the predicted azimuth pattern of the pillbox antenna. The H-plane beamwidth was found to be approximately 3.8° and the first time sidelobes were found to be at a level of -23 dB.

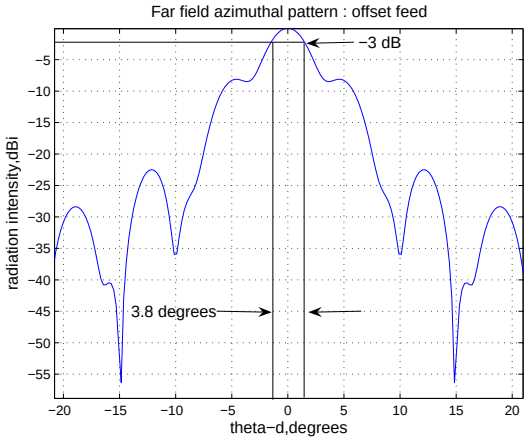

Figure 8: Predicted Azimuth Power Pattern of Pillbox Antenna (offset feed)

Figure 9 shows the MATLAB simulation pattern of the pillbox in the E-plane. The 3 dB beamwidth was found to be 25° and the first sidelobes were at a level of -13 dB.

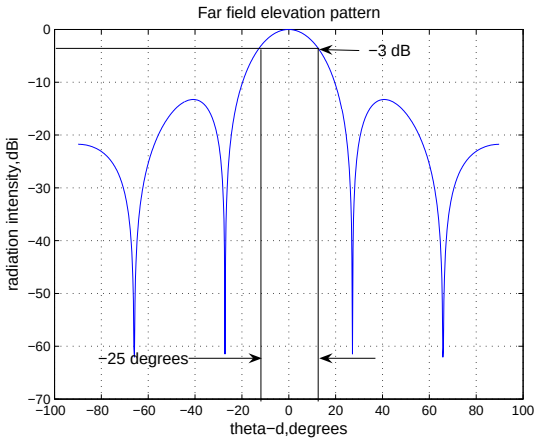

Figure 9: Predicted Elevation Power Pattern of Pillbox Antenna

3.3 Measurement Results

3.3.1 E-plane Pattern

Figure 10 shows the measured E-plane co-polarized pattern as well the cross-polarized pattern.The measured pattern is shown as annotated points. The 3 dB

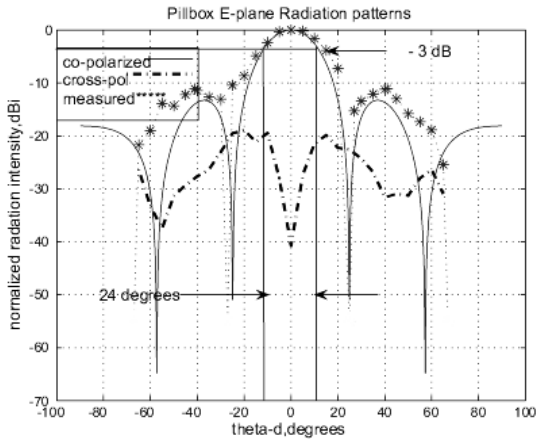

Figure 10: Measured E-plane pattern and cross-pol performance of Pillbox (W.r.t peak gain)

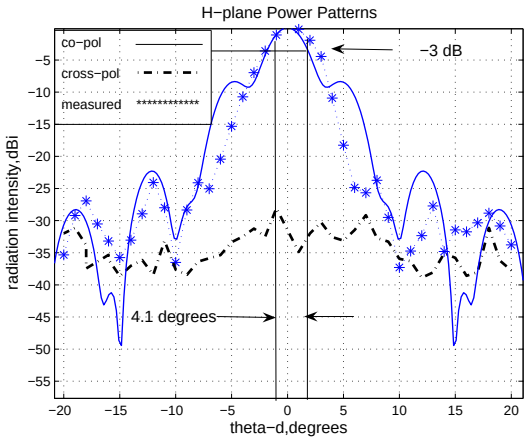

Figure 11: Measured H-plane Pattern and Cross-pol Performance of Pillbox (w.r.t. peak gain)

beamwidth was measured and found to be $24 \pm 0.5^\circ$ in comparison to the predicted value of 25°. The first sidelobe level was found to be approximately -11 dB compared to a predicted value of -13 dB. The antenna offers good cross-polarization rejection in the E-plane (levels less than -30 dBm) within 20° of the beam peak. The peak cross-polarization level was limited to about -22 dBm relative to the peak of the main beam in the E-plane. The noise floor of the receiver was approximately -80 dBm (-60 dB relative to the peak of the main beam co-polarized level).

3.3.2 H-plane Pattern

Figure 11 shows the measured H-plane pattern and the cross polarization performance. The first sidelobe level was found to be approximately -24 dB in comparison to the MATLAB prediction of -23 dB. The measured H-plane 3 dB beamwidth was found to be 4.1° in comparison to the predicted value of 3.8°. This is justified since a wider beam implies lower sidelobes due to the taper imposed on the reflector edges. A maximum cross-polarization level of -28 dBm occurred -3° off the peak of the main beam. The cross-polarization rejection was generally quite good within 20° of the beam peak (less than -30 dBm relative to the peak of the main beam). The noise floor of the receiver was approximately -77 dBm (about 50 dB below the peak of the co-polarized pattern).

3.3.3 Power Gain

We calculated the power gain using equation 21 which is known as the Friis equation [2][8]:

$$\mathrm{G_{t\ dB}} = 20\log_{10}\left(\frac{4\pi \mathrm{R}}{\lambda}\right) + 10\log_{10}\left(\frac{\mathrm{P_r}}{\mathrm{P_t}}\right) - \mathrm{G_{r\ dB}} \quad (21)$$

where

$\mathrm{G_{t\ dB}}$ = gain of transmitting antenna [dB]
$\mathrm{G_{r\ dB}}$ = gain of receiving antenna [dB]
R = antenna separation [m]
λ = operating wavelength of antenna [m]
$\mathrm{P_r}$ = received power [W]
$\mathrm{P_t}$ = transmitted power [W]

We use the Friis equation for a far-field distance of 20 m with a transmit power equal to 20 dBm. We account for all the losses in the measurement system prior to and after taking measurements before calculating the power gain of the antenna. The losses are shown in the loss budget Table 1.

The power gain was calculated to be 24 ± 0.5 dBi compared to a directivity of 25.6 dBi. Where the total uncertainty is the sum of the uncertainties associated with $\mathrm{G_r}$ and $\mathrm{P_r}$. The other quantities in equation 21 above were measured accurately before and after the experiments and they stayed the same.

Table 1: **Losses in Measurement System**

Loss of transmitter (before and after)	1 dB
Insertion loss of transmitting cable	2 dB
Insertion loss of receiving cable	2 dB

4 Conclusions

This paper described the design, implementation and testing of the pillbox antenna for SASARII. The antenna is designed according to the specifications given at the beginning of the paper.

The antenna simulations in MATLAB gave the predicted E and H-plane patterns of the feed and the pillbox. The beamwidth of the antenna and the directivity were computed from the radiation patterns.

The fully fabricated antenna was tested and the results of the tests suggested that the antenna performed satisfactorily and within the specifications. In summary the measured azimuth beamwidth was found to be 4.1° and the elevation beamwidth was found to be 24°. The predicted E and H-plane beamwidths were 3.8° and 25° respectively. The power gain was measured and found to be 24 ± 0.5dBi. The cross-polarization rejection was generally quite good within the main beam for both the E and H-plane measurements; X-pol measurements were less than -30 dB relative to the pattern peaks.

The slightly wider H-plane measured beamwidth could have been due to improper focussing of the feed. The feed exhibits both lateral and axial movement as it is moved back and forth in trying to locate the phase centre. A remedy to this might be to find a way of making the axial and lateral movements independent whilst attempting to find the phase centre. There is also a discrepancy between the general shape of the predicted and the measured H-plane patterns. Both Figure 8 and Figure 11 have nulls at $\pm 10^\circ$, $\pm 15^\circ$ $\pm 20^\circ$ but the measured pattern has a 10 dB beamwidth of 8° while in the predicted pattern it is 12°. This discrepancy could be due to a quadratic phase error at the aperture of the pillbox or an error in programming Equation 10 to obtain the predicted radiation pattern.

Acknowledgements

The authors would like to thank colleagues in the RRSG, the project sponsors and the examiner of S. Gambahaya's dissertation, for all their contributions towards the research. Special thanks to Reuben Govender for supplying the CAD for the antenna.

A Appendices

A.1 Method for Determining H-plane 3 dB Beamwidth

This page explains the method for calculating the 3 dB beamwidth of the antenna in the H-plane to an accuracy of 0.1°. The user requirements stated a desired azimuth beamwidth of 3.8°, however since the measurements were carried out manually there was no protractor available that could measure to an accuracy of 0.1°. The method described below might seem crude but it was quite effective in measuring the H-plane beamwidth. The experiment was performed twice and consistently gave the same results.

A.2 Description

We suggest a method based on the small angle approximation:

$$\mathrm{S} = \mathrm{R}\theta$$

Where

$$\begin{aligned} \mathrm{S} &= \text{arc length=distance between dots} \\ \mathrm{R} &= \text{far-field distance} \\ \theta &= \text{Small angular increment} \end{aligned}$$

This method is justified since θ is very small and R is large. See figure 12. The figure simply illustrates the concept and is not at all to scale.

A laser pointer was attached to the top plate of the antenna just above the aperture. We scanned through peak power to 3 dB points and then bisected the subtended angle to find the peak. Having located the boresight we marked it on a chart which was placed in the background of the receiver at the same height as the receiver. The laser beam was used to accurately mark off the position of the peak on the background chart (see figure 12). With the peak position as reference, the total subtended angle to the 3 dB points was measured by shining the laser to those points and recording the distance between the points.

The distance between the dots corresponding to an angle of 0.1° is given by:

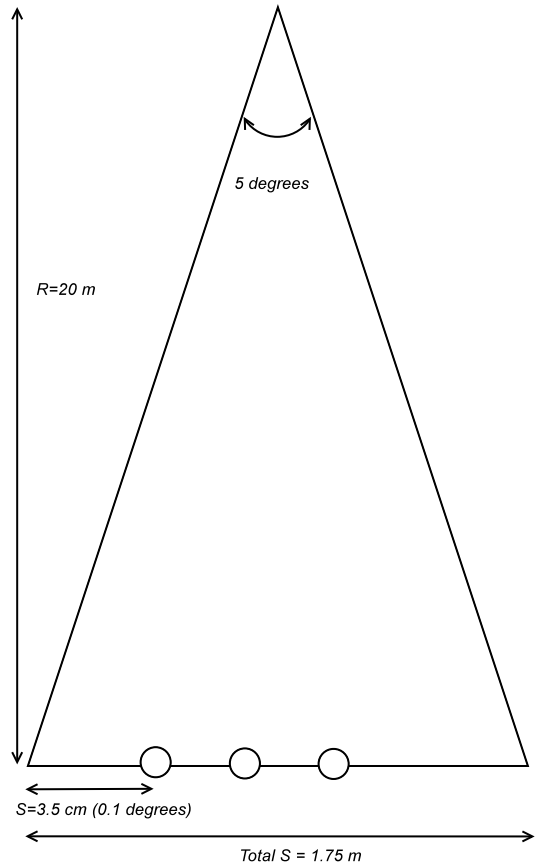

Figure 12: Construction for Determining 3 dB Points

$$\begin{aligned} \mathrm{S} &= \mathrm{R}\theta \\ &= 20 \times \left(\frac{0.1 \times \pi}{180}\right) \\ &= 3.5 \ [\mathrm{cm}] \end{aligned}$$

Using this method the beamwidth was measured accurately to be $4.1°$.

Figure 13: Receive horn with the 'dotted' background chart

B Feed Angle for Equal Edge Illumination

This section shows how the feed pointing angle for equal edge illumination was obtained using a graphical method which will be illustrated shortly. The design is based on finding an angle which gives a feed taper imbalance that corresponds to an equal edge illumination.

The difference in edge illumination at the edge of the reflector is given by [20] :

$$\Delta\mathrm{EI} = \mathrm{EI_U} - \mathrm{EI_L} \ [\mathrm{dB}] \quad (22)$$

For a balanced edge illumination $\Delta EI = 0$, therefore equation 22 can be written as [20]:

$$\mathrm{FT_L} + \mathrm{SPL_U} = \mathrm{FT_L} + \mathrm{SPL_L} \quad (23)$$

Substituting SPL into equation 22 gives

$$\begin{aligned} \Delta\mathrm{FT} &= \mathrm{FT_L} - \mathrm{FT_U} \quad (24) \\ &= 40 \log \left[\frac{\cos\frac{\psi_\mathrm{L}}{2}}{\cos\frac{\psi_\mathrm{U}}{2}}\right] \\ &= 4.5 \ [\mathrm{dB}] \end{aligned}$$

Therefore $\Delta\mathrm{FT} = 4.5$ dB.

The angle between the lower and the upper edge of the reflector is approximately equal to $69°$.

B.1 Description

A Small piece of gridded paper is cut out with the same scale as in the feed pattern and with a width of $69°$. The reference points 'O' and $\Delta\mathrm{FT}$ are marked as shown in figure 14. The marked piece of paper is moved on the feed radiation pattern plot until the points 'O' and $\Delta\mathrm{FT}$ fall on the feed pattern curve. Finally the value of the angle between the pattern peak and the lower edge point $\Delta\mathrm{FT}$, is read from the graph [20] .

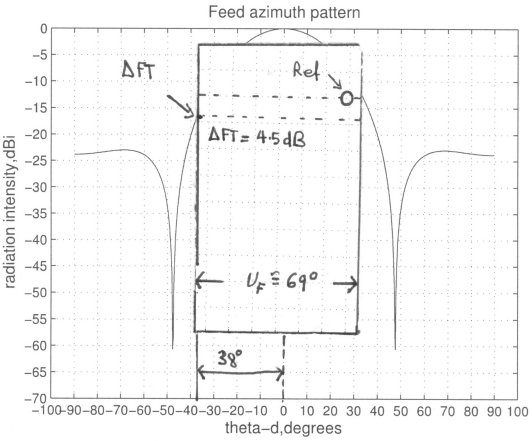

Figure 14: Feed Pointing Angle for Equal Edge Illumination

The feed pointing angle is then calculated by adding ψ_L to ψ_P. For this antenna the feed pointing angle for equal edge illumination was calculated to be:

$$\begin{aligned} \psi_\mathrm{E} &= \psi_\mathrm{L} + \psi_\mathrm{P} \\ \psi_\mathrm{E} &= 11° + 38° \\ &= 49° \end{aligned} \tag{25}$$

References

[1] *IEEE Standards Online Antennas and Propagation Standards*.

[2] Balanis C A. *Antenna Theory: Analysis and Design*. John Wiley and Sons, 1997.

[3] Bracewell R. *The Fourier Transform and its Applications*. McGraw-Hill Book Company, Jan 1965.

[4] Chang K. *RF and Microwave Wireless Systems*. John Wiley and Sons, 2000.

[5] Clarke R H, Brown J. *Diffraction Theory and Antennas*. John Wiley and Sons, Jan 1980.

[6] Elliott R S. *Antenna Theory and Design*. Prentice Hall, Jan 1981.

[7] Harris F J. On the Use of Windows for Harmonic Analysis with the Discrete Fourier Transform. *IEEE Proceedings*, 66(1):51–83, Jan 1978.

[8] Hollis J.S. *Microwave Antenna Measurements*. Scientific-Atlanta, Inc, Atlanta Georgia, Jul 1979.

[9] Holzman L. Pillbox Antenna Design for Millimeter Wave Base-station applications. *IEEE Antennas and Propagation Magazine*, Vol.45(1):30–37, Feb 2003.

[10] Inggs M R. SASAR II Design Document. Technical report, University of Cape Town - RRSG, 2003.

[11] Inggs M R. SASAR II Subsystem Requirements. Technical report, University of Cape Town - RRSG, 2003.

[12] Inggs M R. SASAR II User Requirements. Technical report, University of Cape Town - RRSG, 2003.

[13] Jasik H, Johnson R C. *Antenna Engineering Handbook*. McGraw-Hill Book Company, 1961.

[14] Jefferies D. MSc antennas laboratory. http://www.ee.surrey.ac.uk/Personal/D.Jefferies/antmeas.html, Mar 1998.

[15] Kraus J D. *Antennas*. McGraw-Hill Book Company, 2nd edition, 1997.

[16] Orfanidis S J. Electromagnetic Waves and Antennas. The book should be published by the end of 2004, 2004.

[17] Pozar D M. *Microwave and RF Design of Wireless Systems*. John Wiley and Sons, 2001.

[18] Rudge A W, Adatia N A. Offset-Parabolic-Reflector Antennas: A Review. In *Proceedings of the IEEE*, volume 66, pages 1592–1618. Institute of Electrical and Electronic Engineers, 1978.

[19] Silver S. *Microwave Antenna Theory and Design*. McGraw-Hill Book Company, 1949.

[20] Stutzman W, Terada T. Design of Offset-Parabolic-Reflector Antennas for Low Cross Pol and Low Sidelobes. *IEEE Antennas and Propagation Magazine*, 35(6):46–49, Dec 1993.